Journal of The Electrochemical Society, **160** (6) D212-D217 (2013)
0013-4651/2013/160(6)/D212/6/$31.00 © The Electrochemical Society

Anodic Electro Deposition of CeO_2 and Co-Doped CeO_2 Thin Films

M. Santamaria,[a,*,z] L. Asaro,[a] P. Bocchetta,[b] B. Megna,[a,c] and F. Di Quarto[a,*]

[a]*Electrochemical Material Science Laboratory, DICAM, Facoltà di Ingegneria, Università di Palermo, 90128 Palermo, Italy*
[b]*Dipartimento di Ingegneria dell'Innovazione, Università del Salento, via Monteroni, 73100 Lecce, Italy*
[c]*Laboratorio di Materiali per Il Restauro e la Conservazione, DICAM, Facoltà di Ingegneria, Università di Palermo, 90128 Palermo, Italy*

CeO_2 and Co containing CeO_2 thin films were deposited on indium tin oxide and stainless steel by anodic electrodeposition. Scanning electron microscopy showed that the films are flat and show globular morphology and cracks resulting from volume shrinking. According to XRD and Raman Spectroscopy pure ceria layers are crystalline, while the presence of Co induces the formation of amorphous films. The good adhesion and the compactness allowed the photoelectrochemical characterization of the films. A band gap value of 2.9 eV was estimated for CeO_2, while slightly higher values (∼3.0 eV) were estimated for Co containing films. A mechanism for ceria anodic electrodeposition is proposed and discussed.
© 2013 The Electrochemical Society. [DOI: 10.1149/2.065306jes] All rights reserved.

Manuscript submitted January 30, 2013; revised manuscript received March 7, 2013. Published March 21, 2013.

As a functional rare earth oxide with excellent physical and chemical properties, CeO_2 is extensively used in catalyst, fuel cells, UV blockers, ceramics, oxygen storage capacitors and sensors.[1–10] Owing to the wide range of possible applications a large number of works in the past has been devoted to study the processing techniques able to produce ceria thin films. Among the other electrochemical deposition is an attractive method for the synthesis of several materials, since it allows to work in mild conditions (low temperature, atmospheric pressure) and to get materials with controlled composition.

The most common electrochemical process to deposit transitional metal and rare earth oxides is the electrogeneration of base.[11–13] This techniques consists in inducing a pH increase on the electrode surface due to a cathodic polarization of the electrode in presence of species whose reduction is accompanied by OH^- production. A high (local) concentration of hydroxyl ions induces the precipitation of the metal oxide. This cathodic electrodeposition method, successfully employed to prepare well definite ceria-based nanostructures inside the pores of alumina oxide membranes,[14–17] brings to the formation of powdered films on flat substrates showing a very poor adhesion to the electrodes. In order to overcome this problem, in this work we prepared ceria based thin films by employing the anodic electrodeposition method previously proposed in Ref. 18, where CeO_2 layers are grown on stainless steel by oxidizing Ce(III) into Ce(IV) containing species. In order to check the possibility to deposit mixed oxides, we performed the anodic electrodeposition in electrochemical bath containing another metal cation, i. e. Co^{2+}, susceptible to be also oxidized and, thus, giving the possibility to prepare cobalt-cerium oxides co-catalysts which are reported to show good catalytic activity toward the oxidation of hydrocarbons and carbon monoxide.[19–24] The morphology, composition and structural features of the deposited films were characterized ex situ by X-ray diffraction, Raman Spectroscopy and Scanning Electron Microscopy. Thanks to the good adhesion between the deposited layers and the substrate, it was possible to perform in situ photoelectrochemical experiments allowing to estimate the band gap value of the films. Finally, the mechanism of CeO_2 anodic electrodeposition is discussed on the basis of the overall experimental findings.

Experimental

Stainless steel AISI 304 and ITO (Indium tin oxide conducting glass) electrodes were used as substrate for anodic deposition of CeO_2 film. A classic three-electrode cell was employed. Stainless steel foil was used as counter electrode and a saturated Ag/AgCl electrode as reference. The solution consisted of 0.1 M of $Ce(NO_3)_3$, 0.1 M acetic acid and NaOH to adjust pH at ∼7.5 in deionized water. The deposition of Co-doped ceria was performed by adding to solution $Co(NO_3)_2$.

The anodic polarization was performed at 70°C in galvanostatic regime using a multichannel potentiostat VMP2 (Princeton Applied Research). Before each experiment, the ITO and AISI (after mechanically treatment with abrasive paper up to 1200 grit) were sonicated in acetone.

The annealing process of the ceria-based films was carried out under air exposure by increasing temperature from 25°C to 450°C, keeping this temperature for 20 min and leaving samples cooling inside the furnace.

Morphology and quality of the films were investigated by using a Philips XL30 ESEM Scanning Electron Microscope (SEM). X-ray Diffraction (XRD) analysis was realized by a Philips X-Ray Generator (Model PW 1130) and a PW (Model 1050) goniometry. Micro Raman analysis were performed through a Renishaw inVia Raman Microscope spectrometer equipped with a microprobe (50×) and a CCD detector with a Nd:YAG laser of 532 nm.

The photoelectrochemical experiments were performed in 0.1 M NaOH electrolyte using platinum wire as counter electrode and saturated Ag/AgCl as reference electrode. The experimental set-up employed for the photo-electrochemical investigations is described elsewhere.[25] It consists of a 450 W UV-Vis Xenon lamp coupled with a motorized monochromator (Kratos), which allows monochromatic irradiation of the specimen surface through the electrochemical cell quartz windows. A two-phase lock-in amplifier (EG&G) was used in connection with a mechanical light chopper (frequency: 13 Hz) in order to separate the photocurrent from the total current circulating in the cell.

Results

Electrodeposition.— In Fig. 1a we report the potential of the working electrode vs time during anodic polarization at 0.5 mA cm^{-2} at 70°C of stainless steel in Ce^{3+} and Ce^{3+}/Co^{2+} containing solutions. When cerium ions are present in the electrolyte, the potential raises quickly to ∼1 V and keeps almost constant for all the deposition time. When only Co^{2+} ions are present the electrode potential is sensitively lower (∼0.6 V) and the deposition leads to the formation of very cracked films with very poor adhesion. When the same process is performed on ITO (see Fig. 1b), the dependence of potential on time is slightly different. In contrast to the almost constant potential values measured during the polarization of SS, the overvoltage necessary for sustaining the imposed constant current is higher with respect to the corresponding values on SS and (especially in the case of Co^{2+} free electrolyte) increases during the deposition.

As will be deeply discussed below, the anodic process associated to the imposed current is the oxidation of Ce^{3+} to form CeO_2 and/or of Co^{2+} to form Co_3O_4 and Co_2O_3.

As reported in the literature for the anodic electrodeposition of inorganic oxides,[26] at the employed current density we expect a low

*Electrochemical Society Active Member.
[z]E-mail: monica.santamaria@unipa.it

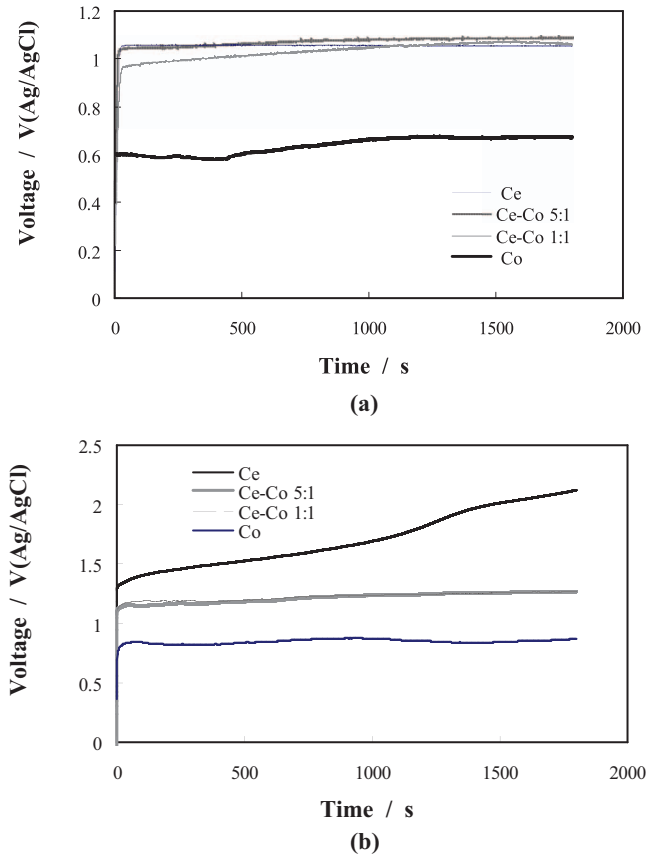

Figure 1. Potential vs time curves recorded during anodic polarization at 0.5 mA cm^{-2} at 70°C in Ce^{3+} and Ce^{3+}/Co^{2+} containing solutions. Working electrode: a) stainless steel and b) ITO.

nucleation rate, leading to the formation of only a few oxide nuclei on the electrode surfaces during the initial stages (1–2 s) of electrodeposition. Thus, a continuous layer is not formed initially on the surface and oxide particles serve as seeds for the growth of the globules evidenced thanks to the morphological characterization (see below).

Structural and morphological characterization.— In Fig. 2 the X-ray diffraction (XRD) patterns relating to films deposited from a Ce^{3+} containing solution at 0.5 mA cm^{-2} before and after the thermal treatment on SS are reported. The peaks relating to AISI 304 substrate are also indicated in the figure for comparison. In both cases the deposits revealed peaks that can be ascribed to CeO_2 (ICCD cards

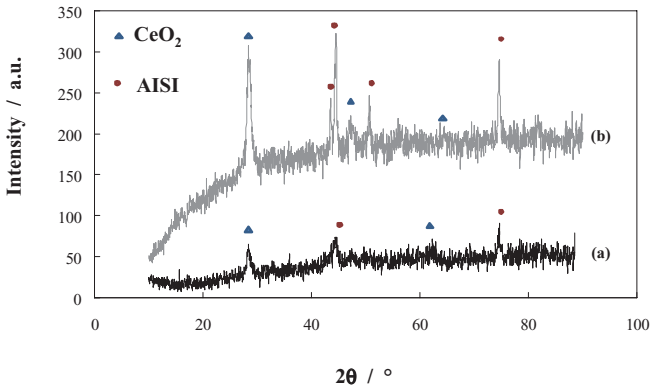

Figure 2. X-ray diffraction patterns relating to films deposited on SS at 70°C from a Ce^{3+} containing solution at 0.5 mA cm^{-2} before (a) and after (b) the thermal treatment.

34-0394 and 01-0880). It can be observed that soon after preparation the deposited materials have a certain quantity of amorphous phase, whereas after thermal treatments (20 min at 450°C under air exposure) the crystallinity is enhanced (see Fig. 2). It is interesting to mention that in the XRD pattern relating to the film deposited galvanostatically on ITO the peaks attributed to CeO_2 are not so evident, thus suggesting the formation of a less crystalline and/or thinner layer.

From XRD characterizations, Co-doped ceria film before and after thermal treatment at 450°C for 20 min appeared amorphous. For oxides prepared from Ce/Co 1/1 molar ratios only the peaks of AISI 304 substrate are revealed before and after thermal annealing at 450°C. Similar results have been obtained for films electrodeposited from Ce/Co 5/1 molar ratios and Co^{2+} containing solutions. This finding indicates that cobalt (II) ions sensibly affects the crystalline structure of CeO_2 and it can be interpreted as an indication that the deposition process brings to the formation of an amorphous mixed oxide phase, in agreement with previous experimental findings on the cathodic deposition of Ce-Co mixed oxides nanotubes.[14]

In Fig. 3a and 3b we report the Raman spectra relating to as-prepared and thermal treated films deposited galvanostatically on SS. Cerium dioxide of fluorite type structure has a single allowed triply degenerate Raman active mode of F_{2g} symmetry, representing the symmetrical stretching vibration of CeO_8 vibrational unit. The Raman peak at 456 cm^{-1} in the spectra of Fig. 3a, is reported to correspond to this mode for not calcined ceria particles. A shift toward higher wavenumber can be evidenced after high temperature annealing (see Fig. 3b) for both ceria and Co-containing ceria that is usually attributed to a higher degree of crystallinity and/or increase in crystallite size [Ref. 16, 17 and refs. therein], as further supported by the increase in

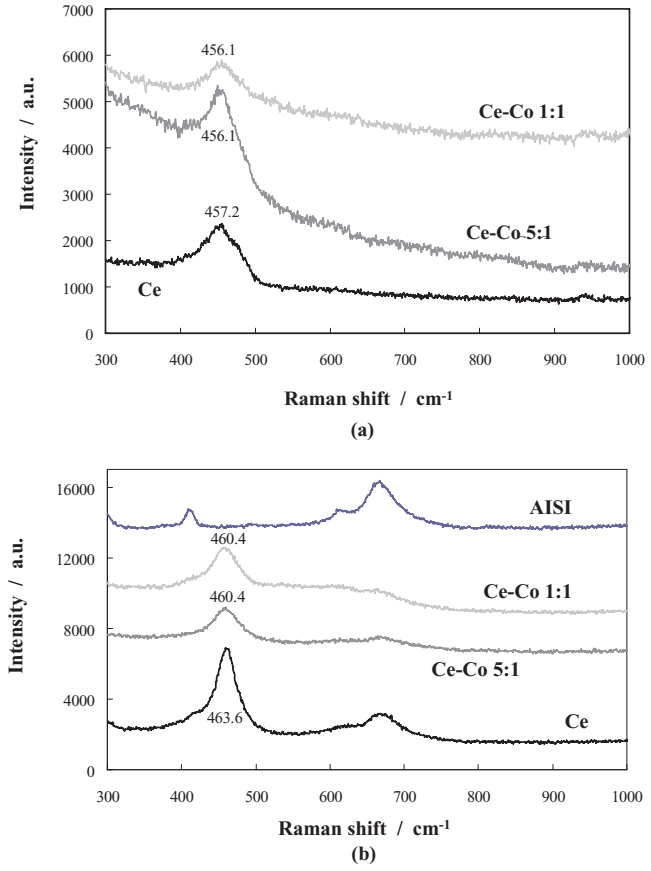

Figure 3. Raman spectra relating to as-prepared films deposited at 0.5 mA cm^{-2} on SS at 70°C from a Ce^{3+} and/or Co^{2+} containing solution (overall metal cation concentration $[Ce^{3+} + Co^{2+}] = 0.1$ M) before and after the thermal treatment.

the symmetry of the Raman band and by the decrease in the full width at half maximum as a consequence of the thermal treatment (compare Fig. 3a and 3b). However, the Raman peak occurs at 463 cm^{-1} for CeO_2 and at 460 cm^{-1} for cobalt containing cerium oxide. This shift of the F_{2g} mode to lower frequencies is reported to occur in doped samples, thus can be interpreted as an indication that Co is effectively incorporated inside the CeO_2 structure. Moreover, this Raman band appears broader for Co containing oxides, thus suggesting the formation of a less crystalline phase in agreement with the XRD results. The substitution of Ce^{4+} with aliovalent cations (Co^{3+} and/or Co^{2+}) allows ceria doping, i. e. an increase of oxygen vacancies concentration as described by the following substitution reactions in Kroger–Vink notation:

$$CoO \xrightarrow{CeO_2} Co''_{Ce} + V_O^{\bullet\bullet} + O_O^X$$

$$Co_2O_3 \xrightarrow{CeO_2} 2Co'_{Ce} + V_O^{\bullet\bullet} + 3O_O^X$$

This substitution introduces distortion in the lattice due to sensitively difference in the ionic radius. According to the literature,[27] $r_{Co^{2+}} = 0.745$ Å and $r_{Co^{3+}} = 0.61$ Å, while $r_{Ce^{4+}} = 0.97$ Å, thus a lattice contraction is expected as a consequence of cobalt oxide co-precipitation.

In Fig. 4 we compare the SEM micrographs relating to ceria films deposited at 0.5 mA cm^{-2} for 30 min on SS (a, b) and ITO (c, d). The layers deposited on AISI show a smooth surface with the presence of very pronounced cracks (see Fig. 4a). At higher magnifications, the deposits appear constituted by nanometric-sized particles, with diameters in the order of 10–20 nm (see Fig. 4b). If the deposition is performed in the same electrochemical conditions but on ITO the deposited layers appear more compact (see Fig. 4c) with respect to those obtained on SS, but with morphological features at the nano-scale very similar to those shown by films on SS, as it can be appreciated at higher magnifications (see Fig. 4d). The formation of a less cracked film on ITO is in agreement with the more anodic potential measured during the electrodeposition with respect to SS. The whole potential drop that sustains the electrochemical reactions must include a contribution inside the growing layer, which covers the conducting substrates more effectively with respect to stainless steel.

In Fig. 5 we report the SEM micrographs relating to Co-coped ceria films grown on SS (a, b) and ITO (c, d). Looking at the films' surface

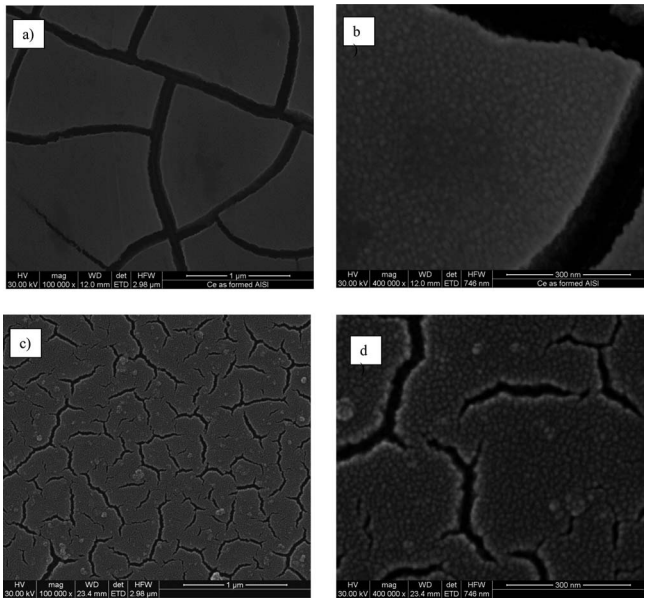

Figure 4. SEM micrographs relating to ceria films deposited at 0.5 mA cm^{-2} for 30 min on SS (a, b) and ITO (c, d).

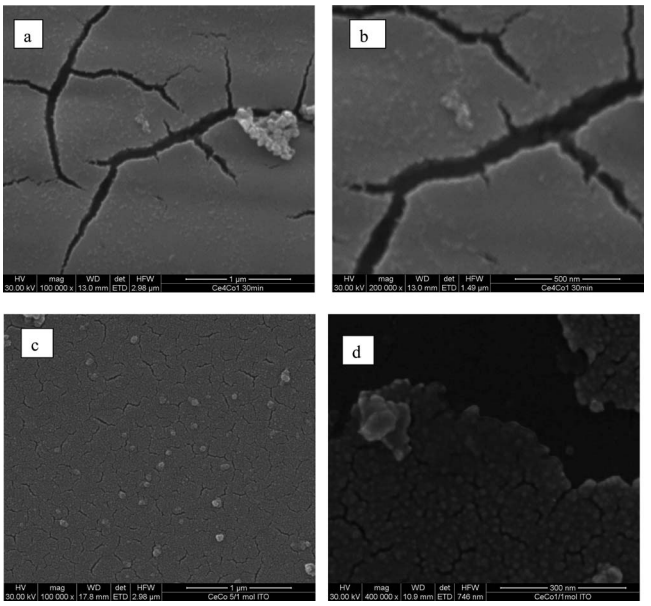

Figure 5. SEM micrographs relating to films deposited from a solution with $Ce^{3+}/Co^{2+} = 5/1$ at 0.5 mA cm^{-2} for 30 min on SS (a, b) and ITO (c, d).

at lower magnification, it seems that the presence of cobalt brings to the formation of less cracked deposits on both the investigated substrates (compare Fig. 4a and 4c with Figs. 5a and 5c). However, at higher magnification the surfaces appear constituted by nanospheres very similar to those constituting pure ceria layers. The EDX analysis performed on the investigated samples confirmed the presence of cerium in the deposit. The Co identification in the doped sample was not possible for films on SS, since Co peaks are masked by Fe peaks of the substrates. The EDX analysis of doped ceria deposited on ITO confirmed the presence of Co (see Fig. 6).

Photoelectrochemical characterization.— Photoelectrochemical experiments were performed with electrodeposited films on ITO substrates. Due to the photoactivity of stainless steel, it is not possible to discriminate between the photocurrent generated by optical transitions involving the deposited material and the photocurrent coming from the films formed on SS especially after annealing.

The photoelectrochemical characterization was carried out in 0.1 M NaOH solution (pH 13). At this pH at room temperature CeO_2 is thermodynamically stable according to the Pourbaix diagram relating to Ce-H_2O.[28] The films resulted photo-active, thus suggesting a good adhesion with the substrate in contrast to the behavior of ceria films deposited via cathodic electrogeneration of base.

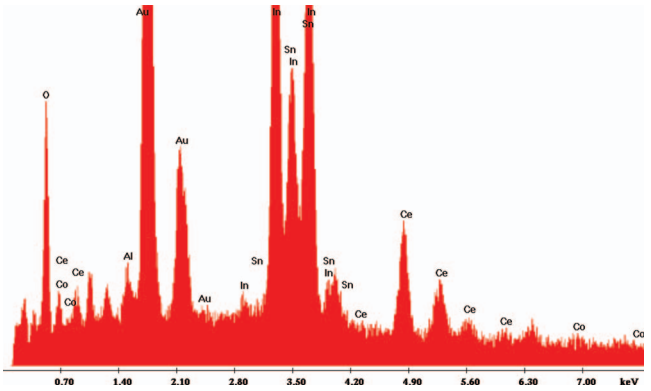

Figure 6. EDX spectrum relating to film deposited from a solution with $Ce^{3+}/Co^{2+} = 1/1$ at 0.5 mA cm^{-2} for 30 min on ITO.

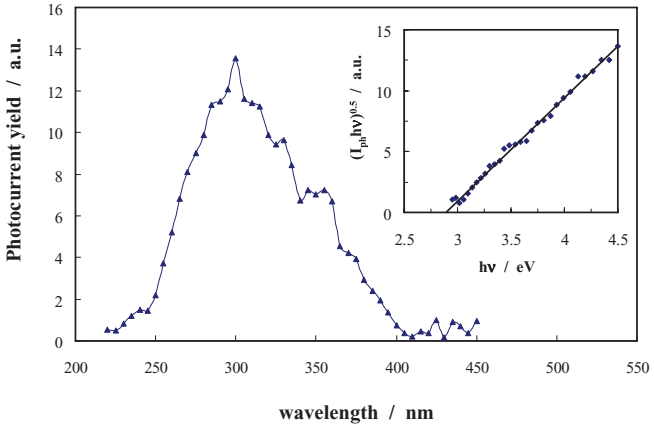

Figure 7. Photocurrent spectrum relating to ceria film deposited at 70°C and 0.5 mA cm^{-2} for 30 min on ITO, annealed for 20 min at 450°C, recorded by polarizing the electrode at 0.4 V vs (Ag/AgCl) in 0.1 M NaOH. Inset: band gap estimate under the hypothesis of non direct optical transitions.

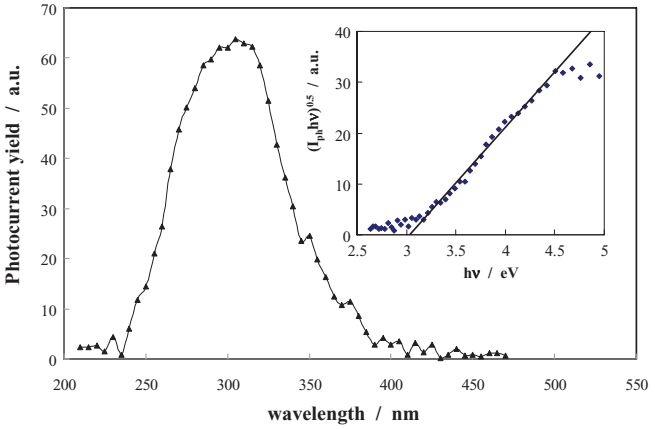

Figure 9. Photocurrent spectrum relating to film deposited from a a solution with Ce^{3+}/Co^{2+} = 5/1 at 70°C and 0.5 mA cm^{-2} for 30 min on ITO, and then annealed at 450°C, recorded by polarizing the electrode at 0.4 V vs (Ag/AgCl) in 0.1 M NaOH. Inset: band gap estimate under the hypothesis of non direct optical transitions.

In Fig. 7 we report the photocurrent spectrum relating to the film deposited galvanostatically at 0.5 mA cm^{-2} for 30 min on ITO and annealed at 450°C for 20 min, recorded by polarizing the electrode at 0.4 V vs (Ag/AgCl) in 0.1 M NaOH. The optical band gap was estimated according to the equation:

$$(I_{ph}h\nu) \propto \left(h\nu - E_g^{opt}\right)^n$$

where I_{ph} is the photocurrent yield, proportional to the light absorption coefficient, hν is the photon energy and the exponent n depends on the kind of optical transitions occurring under irradiation.[25] By assuming non direct optical transition (n = 2), an optical band gap around 2.9 eV can be estimated (see inset), which is lower than the band gap usually reported for bulk ceria (3.2 eV) generated by transitions from the O 2p to Ce 4f orbitals. However, this red-shift has been already reported for thin CeO_2 films in Ref. 29, where quantum confinement effects arising from the reduction of one dimension of the prepared structure to the nanometric scale does not cause the undesired blue shift, thanks to the increased concentration of oxygen vacancies and, more generally, of defects whose presence overcomes the expected influence of the regular quantum size effect.

In order to get information on the sign of the generated photocurrent we performed manually chopped experiments, recording the current under the dark and under irradiation at constant wavelength (see Fig. 8). The photocurrent was anodic at all the investigated wavelengths. The unchopped I_{ph} is higher (29 nA at λ = 300 nm) than that recorded under chopped light (13 nA at λ = 300 nm): their ratio is $\sim\frac{\pi}{\sqrt{2}}$, as expected due to the use of the lock in amplifier for recording photocurrent spectra.[30] Non sensitive improvement of the electrode performance was achieved as a consequence of the annealing.

In Fig. 9 we report the photocurrent spectrum relating to a thin film deposited on ITO for 30 min from a solution with a Co/Ce = 1/5 after thermal treatment, recorded at 0.4 V(Ag/AgCl) in 0.1 M NaOH. The photoelectrochemical characterization before annealing was not possible due to the high current circulating in the cell in the dark. Also in this case the photocurrent was anodic at all the investigated wavelengths (see Fig. 10). Higher photocurrent values were recorded with respect to undoped CeO_2 in presence of the slightly larger optical band gap value (E_g^{opt} = 3.0 eV). The slightly larger optical band gap can be attributed to the amorphous nature of the films evidenced by XRD and Raman results. As discussed in previous work[25] and in agreement with Mott and Davis model of density of states distribution in amorphous semiconductors, larger E_g^{opt} can be explained by the presence of localized states near the mobility edges of SC.

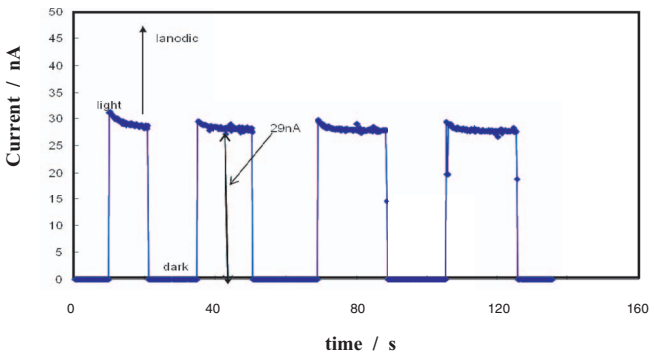

Figure 8. Total current vs time recorded at 0.4 V Ag/AgCl in the dark and under illumination (λ = 300 nm) for CeO_2 film of Fig. 7.

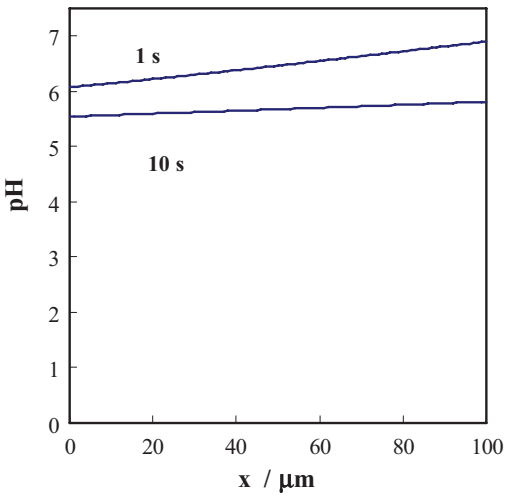

Figure 10. pH profiles expected at the early stage (t = 1 s and 10 s) of oxidation, calculated taking into account the neutralization reaction with acetate ions. A diffusion coefficient $D_{H^+} = 9.3 \cdot 10^{-5}$ cm^2 s^{-1} was used in Eq. 6, as reported in Ref. 32.

Discussion

The electrodeposition of CeO_2 from a Ce^{3+} solution is usually achieved via a cathodic process, i.e. the electrogeneration of base where the OH^- production due to water and oxygen reduction causes a raise in the electrolyte pH and the subsequent precipitation of $Ce(OH)_3$. A post formation annealing process is employed to convert the Ce(III) hydroxide to CeO_2. Conversely, the anodic electrodeposition of ceria is not as popular as the cathodic route and, as far as we know, just a few works are devoted to the study of the anodic process,[18] that can give the chance of a single step deposition of ceria. This is in part due to the severe conditions that must be employed to perform such process, that occurs under high polarization potential and thus limits the choice of the electrode materials.

According to the experimental results reported in this work, we have successfully deposited ceria on both stainless steel and ITO in the electrochemical bath of Ref. 18, where the reaction mechanism leading to the formation of CeO_2 film consists of a first step with complexation and slow release of Ce(III) ions:

$$Ce^{3+} + xL \rightarrow Ce(III)L_x \,(L \text{ is } CH_3COO^-) \qquad [1a]$$

$$Ce(III)L_x + H_2O \rightarrow Ce^{3+} + HL_x + OH^- \qquad [1b]$$

and a second step of Ce(III) oxidation at the electrode interface with subsequent precipitation of CeO_2:

$$Ce^{3+} + 2H_2O \rightarrow [Ce(OH)_2]^{2+} + 2H^+ + e^- \qquad [2a]$$

$$Ce(OH)_2^{2+} \rightarrow CeO_2 + 2H^+ \qquad [2b]$$

In equation (1) L stands for ligand, i.e. CH_3COO^-, used because the complexation of Ce^{3+} ions favors the stabilization of Ce(III) in solution, preventing Ce_2O_3 precipitation. The release of Ce^{3+} is a slow step (Eq. 1) and it is followed by the charge transfer reaction at the electrode (Eq. 2).

At pH 7.5 assuming $[Ce(OH)_2^{2+}] = 10^{-6}$ M, the equilibrium potential for the reaction 2a calculated according to the following equation:[28]

$$E_{eq} = 1.531 - 0.1182\,pH + 0.059 \log \frac{\left[Ce(OH)_2^{2+}\right]}{[Ce^{3+}]} \text{ V(Ag/AgCl)}$$

depends on free Ce^{3+} concentration. An equilibrium potential ranging between 0.35 V vs Ag/AgCl ($[Ce^{3+}] = 10^{-1}$ M) and 0.65 V vs Ag/AgCl ($[Ce^{3+}] = 10^{-6}$ M) can be calculated, so that at the potential of 1.05 V vs Ag/AgCl recorded during the deposition, reaction 2a is thermodynamically possible. We cannot exclude the occurrence of water oxidation causing O_2 evolution with a subsequent diminution of the faradaic efficiency of the process. If the deposition of CeO_2 occurs via reaction (2) or even if the oxygen evolution reaction takes place, the pH of the deposition bath is expected to decrease due to the H^+ production.

According to the Pourbaix diagram relating to Ce-H_2O system,[28] $[Ce(OH)_2^{2+}]$ is highly soluble in water even in slightly alkaline solution, as suggested by the solubility product of reaction 2b ($K_{SP} = 6 \cdot 10^{-20}$). Thus, at pH 7.5 and taking into account the local acidification expected during the anodic polarization, CeO_2 precipitation according to equation 2b is not plausible. In order to explain how we succeed in depositing CeO_2 in the employed electrochemical bath, we have to consider the updated Pourbaix diagram reported in ref. 31, where the chemical and electrochemical equilibria involving Ce(III) and Ce(IV) compounds in both aerated and not aerated solutions are detailed described, taking into account the possible formation of cerium hydroxo-complexes, i.e. $Ce(OH)_i^{(4-i)+}$, with i ranging between 0 and 4 as a function of potential and pH. The oxidation of Ce(III) to Ce(VI) ions can be described according to the following general half cell reaction:

$$Ce(OH)_i^{(3-i)+} + (4-i)H_2O \rightarrow Ce(OH)_{4,aq} + (4-i)H^+ + e^- \qquad [3]$$

reported to occur with i = 0 when the electrolyte pH is in the range 2.6 – 8.4 on the base of thermodynamic calculation.[31] The experimental evidences arising from titration curves, confirmed that at pH > 4 and in presence of O_2, $Ce(OH)_4$ is the overwhelming species.[31] The equilibrium potential for reaction 3 can be calculated according to the following eq.:

$$E_{eq} = 1.787 + 0.059 \,\text{Log} \frac{[Ce(OH)_4]}{[Ce^{3+}]} - 0.2366\,pH \text{ (V vs Ag/AgCl)}$$

This implies that at pH 7.5 the oxidation of Ce^{3+} ions brings to the formation of $Ce(OH)_4$ that, although initially soluble to some degree in aqueous solution,[31] precipitates as hydrated oxide:

$$Ce(OH)_{4,aq} \rightarrow Ce(OH)_4/CeO_2 \cdot 2H_2O\downarrow \qquad [4]$$

If we assume $[Ce^{3+}] = 0.1$ M and $[Ce(OH)_4] = 1$ M, $E_{eq} = 0.07$ V(Ag/AgCl), thus sensitively more cathodic than the potential measured during the anodic polarization. Even considering negligible the concentration of free Ce^{3+} ions in solution ($[Ce^{3+}] = 10^{-6}$ M) due to the presence of ligand, the equilibrium potential for reaction 3 is 0.37 V vs Ag/AgCl, thus sensitively lower than that measured during the deposition. The described mechanism does not involve directly the ligand. The only role played by acetate is to control the concentration of free Ce^{3+} ions according to Eq. 1a.

In order to account for the local acidification, we tried to calculate the H^+ concentration profiles during the deposition as a function of time and distance from the electrode surface by solving the non stationary Fick's law:

$$\frac{\partial c_{H^+}}{\partial t} = D \frac{\partial^2 c_{H^+}}{\partial x^2} \qquad [5]$$

with the following boundaries conditions:

$$c_{H^+}(t = 0) = 3.1 \cdot 10^{-8} \text{ mol dm}^{-3} \quad \forall x \geq 0$$
$$c_{H^+}(x \rightarrow \infty) = 3.1 \cdot 10^{-8} \text{ mol dm}^{-3} \quad \forall t \geq 0$$
$$J_{H^+} = 2.08 \cdot 10^{-8} \text{ mol cm}^{-2}\text{s}^{-1}$$

where J is the constant flux estimated by assuming that the imposed current density (0.5 mA cm^{-2}) is sustained only by reaction 3 bringing to the production of four hydrogen ions per electron. The analytic solution of Eq. 5 under the hypothesis of constant current density and unitary efficiency is:

$$c_{H^+} = \frac{J_{H^+}}{D^{1/2}} \left[\frac{2\sqrt{t}}{\sqrt{\pi}} \exp\left(-\frac{x^2}{4Dt}\right) - \frac{x}{\sqrt{D}} erfc\sqrt{\frac{x^2}{4Dt}} \right] \qquad [6]$$

If we suppose that all the H^+ produced during the anodic polarization are neutralized by CH_3COO^- ions, we can derive the pH profiles reported in Fig. 10 for the early stages of oxidation (t = 1 s and 10 s). The simultaneous presence of a weak acid (i.e. CH_3COOH) and its conjugate base (i.e. CH_3COO^-) allows the formation of a buffer solution, which controls the acidity of the electrochemical bath and, thus, CeO_2 precipitation.

The pH profiles of Fig. 10 were estimated taking into account only the diffusion contribution to the H^+ transport. If we consider H^+ migration which drives far from the anode hydrogen ions, less acidic solutions are expected, thus not affecting the validity of the proposed reaction scheme for ceria deposition.

We want to finally comment on the co-deposition of cobalt oxide. If the anodic polarization is performed in Co^{2+} containing bath, we have also to take into account the oxidation of cobalt ions to form Co_3O_4 or Co_2O_3, according to the following half cell reactions:

$$3Co^{2+} + 4H_2O \rightarrow Co_3O_4 + 8H^+ + 2e^-$$
$$E_{eq} = 1.912 - 0.2364\,pH - 0.0886 \log\left[Co^{2+}\right] \text{ V(Ag/AgCl)} \qquad [7a]$$

$$2Co^{2+} + 3H_2O \rightarrow Co_2O_3 + 6H^+ + 2e^-$$
$$E_{eq} = 1.546 - 0.1773\,pH - 0.059 \log\left[Co^{2+}\right] \text{ V(Ag/AgCl)} \qquad [7b]$$

For $[Co^{2+}] = 0.1$ M, E_{eq} for the oxidation of Co^{2+} to Co_3O_4 and to Co_2O_3 are 0.228 V and 0.275 V, respectively, both more cathodic than the potential measured during the deposition of pure cobalt oxide. According to the above reported equations, even in the case of the solution most dilute in cobalt (i.e. $[Co^{2+}] = 0.0167$ M), the estimated equilibrium potentials are lower than those measured during the deposition, thus confirming that the electro-precipitation of Co_3O_4 and Co_2O_3 is thermodynamically possible.

Conclusions

The anodic electrodeposition of ceria and Co-doped ceria films was successfully realized on stainless steel and indium tin oxide conducting substrates. By imposing an anodic current density of 0.5 mA cm^{-2}, it is possible to get both pure ceria and Co doped ceria films. According to X-ray diffraction patters and Raman Spectra, pure CeO_2 thin films are crystalline soon after preparation, while Co containing layers appears amorphous even after thermal treatment. Not appreciable differences are induced in the films morphology by Co incorporation, as evidenced by SEM micrographs. The prepared films resulted photoactive and an indirect band gap of 2.9 and 3.0 eV was estimated for pure ceria and Co containing ceria films, respectively. The difference between the band gap values of CeO_2 and Co containing CeO_2 was attributed to the amorphous nature of the latter. On the basis of the experimental findings, a mechanism of CeO_2 anodic deposition is proposed and discussed.

Acknowledgment

The authors thank US Army for the partial financial support under the contract grant W911NF-11-1-0386.

References

1. A. Trovarelli, *Catal., Rev. - Sci. Eng.*, **38**, 439 (1996).
2. R. Dictor and S. Roberts, *J. Phys. Chem.*, **93**, 5846 (1989); E. C. Su and W. G. Rothschild, *J. Catal.*, **99**, 506 (1986).
3. T. Shido and Y. Iwasawa, *J. Catal.*, **136**, 493 (1992); T. Shido and Y. Iwasawa, *J. Catal.*, **141**, 71 (1993).
4. A. Martinez-Arias, J. Soria, J. C. Coneca, X. L. Seoane, A. Arcoya, and R. Cataluna, *J. Chem. Soc. Faraday Trans.*, **91**, 1679 (1995).
5. E. Odier, Y. Schuurman, and C. Mirodatos, *Catal. Today*, **127**, 230 (2007).
6. N. Izu, W. Shin, I. Matsubara, and N. Murayama, *Sens. Actuators B*, **113**, 207 (2006).
7. S. Hilaire, X. Wang, T. Luo, R. J. Gorte, and J. A. Wagner, *Appl. Catal. A*, **215**, 271 (2001).
8. B. Dalslet, P. Blennow, P. V. Hendriksen, N. Bonanos, D. Lybye, and M. Mogensen, *J. Solid State Electrochem.*, **10**, 547 (2006).
9. ZS Duan, M. Yang, Z. Hou, Y. Dong, Y. Chong, M. Cheng, and W. Yang, *J. Power Sources*, **160**, 57 (2006).
10. T. Tsai and S. A. Barnett, *Solid State Ionics*, **98**, 191 (1997).
11. G. H. A. Therese and P. V. Kamath, *Chem. Mater.*, **12**, 1195 (2000).
12. K. Kamada, N. Enomoto, and J. Hojo, *El. Acta*, **54**, 6996 (2009).
13. V. Lair, L. S. Zivkovic, O. Lupan, and A. Ringuuede, *El. Acta*, **56**, 4638 (2011).
14. P. Bocchetta, M. Santamaria, and F. Di Quarto, *Electrochem. and Solid State Letters*, **11**, K27 (2008).
15. P. Bocchetta, M. Santamaria, and F. Di Quarto, *Electrochem. and Solid State Letters*, **11**, K93 (2008).
16. P. Bocchetta, M. Santamaria, and F. Di Quarto, *Journal of Applied Electrochemistry*, **39**, 2073 (2009).
17. P. Bocchetta, M. Santamaria, and F. Di Quarto, *J. Electrochem. Soc.*, **159**, E108 (2012).
18. (a) A. Q. Wang and T. D. Golden, *J. Electrochem. Soc.*, **150**, C616 (2003); (b) T. D. Golden and A. Q. Wang, *J. Electrochem. Soc.*, **150**, C621 (2003).
19. J. Kirchnerova, M. Alifanti, and B. Delmon, *Appl. Catal. A*, **231**, 65 (2002).
20. M. Kang, M. W. Song, and C. H. Lee, *Appl. Catal, A*, **251**, 143 (2003).
21. M. M. Natile and A. Glisenti, *Chem. Mater.*, **17**, 3403 (2005).
22. L. F. Liotta, G. Di Carlo, G. Pantaleo, A. M. Venezia, and G. Deganello, *Appl. Catal. B*, **66**, 217 (2006).
23. C. W. Tang, C. C. Kuo, M. C. Kuo, C. B. Wang, and S. H. Chien, *Appl. Catal. A*, **309**, 37 (2006).
24. L. F. Liotta, G. Di Carlo, G. Pantaleo, and G. Deganello, *Appl. Catal. B*, **70**, 314 (2007)
25. F. Di Quarto, S. Piazza, M. Santamaria, and C. Sunseri, *Handbook of Thin Films*, H. S. Nalwa, Vol. 2, p. 373, Academic Press, San Diego (2002).
26. B. Babakhani and D. G. Ivey, *J. of Power Sources*, **196**, 10762 (2011).
27. S. M. Bukhari and J. B. Giorgi, *Solid State Ionics*, **181**, 392 (2010).
28. M. Pourbaix, *Atlas of Electrochemical Equilibria in Aqueous Solutions*, Pergamon, New York, 1966.
29. A. Corma, P. Atienzar, H. Garcia, and J-Y Chane-Ching, *Nature Materials*, **3**, 394 (2004).
30. M. L. Maede, *Lock in Amplifier: Principles and Applications*, Peter Peregrinus, London, 1983.
31. (a) S. A. Hayes, P. Yu, T. J. O'Keefe, M. J. O'Keefe, and J. O. Stoffer, *J. Electrochem. Soc.*, **149**, C623 (2002); (b) P. Yu, S. A. Hayes, T. J. O'Keefe, M. J. O'Keefe, and J. O. Stoffer, *J. Electrochem. Soc.*, **153**, C74 (2002)
32. J. S. Newman, *Electrochemical Systems*, p. 255, Prentice Hall, Inc., Englewood Cliffs, New Jersey (1991).